

Courtesy of Paula Echeverri. Used with permission.

**EXPANDABLE FOAM IMPACT ATTENUATION FOR SMALL PARAFOIL
PAYLOAD PACKAGES**

**PROJECT PROPOSAL
VERSION III
16.621**

SPRING 2003

AUTHOR: PAULA ECHEVERRI

ADVISOR: CHRISTIAN ANDERSON

PARTNER: JULIE ARNOLD

MAY 13TH, 2003

TABLE OF CONTENTS

<u>LIST OF FIGURES</u>	<u>4</u>
<u>LIST OF TABLES</u>	<u>5</u>
<u>EXECUTIVE SUMMARY</u>	<u>6</u>
<u>1. INTRODUCTION</u>	<u>7</u>
<u>2. OBJECTIVES</u>	<u>7</u>
<u>2.1 HYPOTHESIS</u>	<u>7</u>
<u>2.2 OBJECTIVE</u>	<u>8</u>
<u>2.3 SUCCESS CRITERIA</u>	<u>8</u>
<u>2.4 EXPERIMENT OVERVIEW</u>	<u>8</u>
<u>3. LITERATURE REVIEW</u>	<u>8</u>
<u>4. TECHNICAL APPROACH</u>	<u>12</u>
<u>4.1 EXPERIMENT PLAN</u>	<u>12</u>
<u>4.2 APPARATUS</u>	<u>17</u>
<u>4.3 TEST ARTICLES</u>	<u>19</u>
<u>4.4 TEST MATRICES</u>	<u>20</u>
<u>4.4.1 CRUSH THICKNESS EFFICIENCY TESTS</u>	<u>20</u>
<u>4.4.2 SAFETY MARGIN TESTS</u>	<u>21</u>
<u>4.4.3 PRE-DEPLOYMENT VOLUME MEASUREMENTS</u>	<u>21</u>
<u>4.4.4 MECHANICAL RELIABILITY TESTS</u>	<u>22</u>
<u>5. DISCUSSION OF ERRORS</u>	<u>22</u>
<u>5.1 CRUSH THICKNESS EFFICIENCY</u>	<u>22</u>
<u>5.2 PRE-DEPLOYMENT VOLUME</u>	<u>23</u>
<u>5.3 SAFETY MARGIN TESTS</u>	<u>23</u>
<u>5.4 ADDITIONAL CONSIDERATIONS</u>	<u>24</u>
<u>6. CONSTRUCTION PROCEDURES</u>	<u>24</u>

6.1	DROP TEST RIG	24
6.2	PAYLOAD BOX	26
6.3	SET UP	27
6.4	SAFETY CONCERNS	28
7.	DATA ACQUISITION AND ANALYSIS	28
7.1	MEASUREMENT SYSTEMS	28
7.2	DATA REDUCTION	29
7.2.1	<i>STATIC CRUSH THICKNESS EFFICIENCY TESTS</i>	29
7.2.2	<i>DYNAMIC CRUSH THICKNESS EFFICIENCY TESTS</i>	29
7.2.3	<i>SAFETY MARGIN TESTS</i>	30
7.2.4	<i>PRE-DEPLOYMENT VOLUME OF EFIA</i>	30
7.2.5	<i>DEPLOYMENT RELIABILITY TESTS</i>	30
7.2.6	<i>HYPOTHESIS ASSESSMENT</i>	30
7.3	ERROR ANALYSIS	31
7.3.1	<i>CRUSH THICKNESS EFFICIENCY MEASUREMENT ERRORS</i>	31
7.3.2	<i>PRE-DEPLOYMENT VOLUME MEASUREMENT ERRORS</i>	32
7.3.3	<i>FINAL CUSHION THICKNESS ERRORS</i>	33
8.	PROJECT PLANNING	35
8.1	16.622 SCHEDULE	35
8.2	FACILITIES AND STAFF SUPPORT	36
9.	SUMMARY	36
10.	REFERENCES	38
<u>APPENDIX A: DETAILED DRAWINGS</u>		
<u>APPENDIX B: PARTS LISTS, PURCHASE SPECIFICATIONS AND BUDGET</u>		
<u>APPENDIX C: SAFETY MARGIN CONFIDENCE ANALYSIS</u>		

LIST OF FIGURES

<u>FIGURE 1: INSTAPAK EXPANDING FOAM</u>	<u>7</u>
<u>FIGURE 2: EXPERIMENT PLAN</u>	<u>12</u>
<u>FIGURE 3: PLOT OF DISPLACEMENT VS. COMPRESSIVE FORCE FOR PAPER HONEYCOMB</u>	<u>14</u>
<u>FIGURE 4(A): PAPER HONEYCOMB</u>	<u>19</u>
<u>FIGURE 4(B): EXPANDING FOAM PRODUCT</u>	<u>19</u>
<u>FIGURE 5: PAYLOAD BOX ISOMETRIC VIEW</u>	<u>20</u>
<u>FIGURE 6: UNISTRUT BEAM</u>	<u>25</u>
<u>FIGURE 7: TOP VIEW OF FRAME ASSEMBLY</u>	<u>25</u>
<u>FIGURE 8: TEST RIG DETAIL ISOMETRIC VIEW</u>	<u>26</u>
<u>FIGURE 9: HYPOTHESIS ASSESSMENT BAR GRAPHS</u>	<u>31</u>

LIST OF TABLES

<u>TABLE 1: TEST MATRIX FOR EACH MATERIAL IN CRUSH THICKNESS EFFICIENCY TESTS</u>	<u>21</u>
<u>TABLE 2: TEST MATRIX FOR EACH IMPACT ATTENUATION MATERIAL IN SAFETY TESTS</u>	<u>21</u>
<u>TABLE 3: TEST MATRIX FOR PRE-DEPLOYMENT MEASUREMENTS</u>	<u>21</u>
<u>TABLE 4: TEST MATRIX FOR MECHANICAL RELIABILITY TESTS</u>	<u>22</u>
<u>TABLE 5: 16.622 SCHEDULE</u>	<u>36</u>

Executive Summary

Honeycomb is commonly used to provide impact attenuation to small payloads delivered by Unmanned Air Vehicles (UAVs). This project aims to identify whether an expanding foam product can be implemented as a low-cost impact attenuation device that, unlike paper honeycomb, will occupy a minimal volume onboard a small aircraft. Expanding foam could broaden the applications of small aircraft for remote and quick payload transport, without a dramatic rise in cost as compared to other complex attenuation devices such as airbags or retraction mechanisms.

During the fall term of 2003 a series of tests will be performed to compare expanding foam to paper honeycomb. The impact attenuation materials will be compared in terms of their impact attenuation efficiency, the pre-deployment volume they would occupy in a payload compartment and the reliability of the deployment mechanism.

A drop test rig will be built at the strong wall in the MIT Department of Aeronautics and Astronautics during the first three weeks of the MIT fall term. Some tests will be performed at this test rig while others will be performed at an Instron force press at the MIT Technology Laboratories for Advanced Composites. Testing is expected to be completed within the first seven weeks of the term.

The eighth and ninth weeks of the term will be spent designing an implementation of Instapak Quick expanding foam to an UAV application. However, if time and resources are limited and the design is not completed, the functional requirements for such a design will be determined. This should motivate further research to complete a design and build a prototype in the future.

The estimated budget for the completion of the project is \$560.00. This amount will be spent in the purchase of some parts and instrumentation that have not been found at the MIT Gelb Lab; plus the purchase of the Instapak Quick foam that will be tested, together with the heater that is used to expand the foam.

1. Introduction

One of the applications of Unmanned Air Vehicles (UAVs) under current research is the transport of payloads to be delivered by small parafoils. Parafoils have typical vertical impact velocities of about 15ft/s, but the payloads delivered usually consist of electronic equipment or are otherwise delicate and require the additional protection of impact attenuation at touchdown.

Previous research on the field concentrates on reliable airbags or retraction mechanisms. These devices, however, are expensive relative to the budgets for small payload deliveries. On the other hand, inexpensive impact shock attenuation materials, such as paper honeycomb or crushable foam take up too much volume onboard UAVs. Volume is a predominant concern when dealing with UAVs, which are generally small aircraft and therefore have limitations in terms of payload volume capacity.

The trade-off between cost or reliability on the one hand and volume occupied onboard on the other suggests the opportunity for a new impact attenuation concept for payload deliveries from UAVs. The following document proposes a series of tests to assess whether expanding foam could provide impact attenuation at a reasonable cost and, before being deployed, take up a minimal volume onboard the UAV. Expanding foam is commonly used for packing shipping containers, for example the company SealedAir has developed a product called Instapak®, shown in Figure 1.

2. Objectives

2.1 Hypothesis

Our primary hypothesis is that an expanding foam impact attenuation device (EFIA) will occupy at least 75% less pre-deployment volume than paper honeycomb with a crush thickness efficiency loss of no more than 30%. Our secondary hypothesis is that other

tradeoffs will not exceed an increase in cost of 50% and a decrease in reliability of no more than 10%.

2.2 Objective

Assess the ability of an EFIA to protect a payload having a 50g-impact shock limit from a 15 ft/s vertical descent rate. This assessment will be done by comparing the pre-deployment volume, crush efficiency, cost and reliability of the EFIA device against paper honeycomb.

2.3 Success Criteria

Evaluation of the aforementioned metrics for an EFIA and for paper honeycomb to an accuracy such that the hypotheses can be assessed.

2.4 Experiment Overview

An expanding foam product will be adapted as an EFIA, and then a series of tests will be performed to evaluate the metrics mentioned in the hypotheses for both the EFIA and the paper honeycomb. These tests will include force press tests to measure crush thickness efficiencies, drop tests to evaluate the impact on the payload and deployments of the EFIA device to evaluate the reliability of the mechanism.

3. Literature Review

In order to assess expanding foam as a potential impact attenuation material, it is crucial to specify the type of foam that will better serve this purpose and to validate the tests included in this proposal.

The discussion of cellular plastics on the Handbook of Industrial Materials identifies the ideal foams for shock mitigation¹. Low density, rigid foams crush and therefore dissipate a considerable amount of energy from an impact shock. Semi-rigid foams, on the other hand, absorb more energy that is then transferred (to the payload) through rebound. Since semi-rigid foams recover after impact, they are in fact widely used for shock mitigation, for instance in automotive applications. However, impact attenuation for parafoil payloads requires only one performance which, furthermore, should be as effective as possible.

This reference is also useful insofar as it cites specific low-density rigid foam products and applications. This will be of great value in the market search for a product that can be adapted as an impact attenuation device. Low-density rigid foams include rigid

polyurethane, polystyrene, polyisocyanurate and phenolic. These are used for packaging of heavy industrial components and more widely for thermal insulation, for example in the casing of cold boxes. The book also mentions the use of expandable polystyrene (EPS), which most closely resembles the type of expanding foam impact attenuation material that could be used for this experiment.

The section on instrumented impact tests on The Handbook of Plastics Test Methods provides a high level background that aids the experimental design for this project². Firstly, it points out the wide and valid practice of drop tests to evaluate variables relevant to impact shock. Secondly, it reviews the typical instrumentation necessary to measure these variables. Thus it mentions that accelerometers are easy to implement in drop test configurations to evaluate impact shock. Accelerometer data is directly transmitted to a computer that stores it for later analysis. The rest of the instrumentation mentioned in this reference is not within the scope of this project. Strain gauges, for instance, will yield a measurement that is directly related to a potential form of energy in an impacted material. As discussed above, this experiment is mostly concerned with materials that dissipate rather than absorb impact energy.

An important consideration for the sampling of data from instruments such as accelerometers is also mentioned here. Given that the time lapse over which impact takes place is so brief, there is the risk of damping the signal of the force-measuring device during sampling. The rule cited is that data points should be gathered at a frequency of $5/t_f$ where t_f is the ‘minimum time to failure that is required to be measured.’ This consideration has in fact been included in the error analysis section of this proposal, where the critical interval is taken to be the material crush time.

Having established some guidance in terms of material selection and test methods, an evaluation of current technology in the field of impact attenuation is appropriate. The existing literature in this field is mostly concerned with larger budget, complex impact attenuation devices such as airbags and retraction mechanisms. Both methods are very effective in terms of protecting payloads with more constraints on damage due to impact shock and they also serve multiple functions within the soft landing system they are part of. However, the increased budget and the bulk taken up by these devices disqualify them for

use in small UAV applications. The motivation behind this experiment lies very heavily on these considerations.

Gardinier et al. give a valuable overview of a typical airbag impact attenuation system in the paper titled “Design and Testing of the HOPE-X HSFD-II Landing System”³. The paper reports on a series of experimental tests and computer simulations performed to aid in the design of the soft-landing system of an unmanned re-entry space vehicle (HOPE-X.) The final design was indeed successful despite some concern about the space allocation of the landing system within the vehicle.

The most straightforward difference between this type of impact attenuation and an EFIA is the mechanical complexity of the airbag system. The two intricate components of the HOPE-X airbag system are a drogue gun deployment mechanism and the controls of the gas vents that monitor the pressure in the airbags. Furthermore, the airbags are part of an even larger, integrated system for soft landing. Some of the tests reviewed in this paper involve the evaluation of the integrated behavior of subsystems that is well beyond the scope of this project.

Upon considering the differences between an airbag landing system and an EFIA, it is easy to understand why there exists more literature on the former. The HOPE-X airbags, for instance, are multifunctional since they also serve to ensure that the payload lands in the correct orientation. These airbags also can protect payloads from impact shocks above 6g, thus providing much more attenuation than a simple crushable material. The complexity of the system also allows for additional safety measures to monitor the performance of the airbags. For instance, even though the airbag is designed within a nominal constraint, a particular trigger exists that liberates some of the gas in the airbags if a certain deceleration level is exceeded.

There are two main things in this paper that aid the motivation of this 16.62X project and the validation of its experimental approach respectively. The first point is the emphasis made on space allocation for the landing system. The motivation for the development of an expandable impact attenuation device is therefore relevant to current concerns in the field. The second point is that the empirical context in which tests of the performance of airbags for impact attenuation take place is very similar to the one discussed in this proposal. Impact velocity is a key parameter for the tests and the

deceleration of the center of gravity of the HOPE-X vehicle is the main concern. Furthermore, the principal objective of the drop tests is to ‘establish confidence’ about the ability of the airbag system to protect the payload from the impact shock limit for which the airbag was designed. The drop tests that will be performed in this 16.62X experiment will similarly allow us to determine a safety margin that the design of an EFIA will take into account to ensure the impact shock limit of the payload is not exceeded.

As mentioned above, the other technology that has been pursued for the purpose of impact attenuation has been retractable mechanisms. Among these, Brown, Haggard and Benney discuss pneumatic muscle actuators (PMA’s).⁴ In this case, PMA’s are used to enhance the soft landing of heavy cargo such as military vehicles.

The paper reviews the PMA force equation that has been developed to calculate the tensile force of the actuators on the payload as they retract. The validity of this equation was compared to empirical results of both static tests and dynamic drop tests, and then a finite element computational method was suggested as an aid in the design of PMA’s for future applications. Overall the results of the tests showed only a minor shortcoming of the analytical model: the PMA force equation failed to account for the fact that the retraction of the actuator produces a pull downward on the parafoil besides the pull upward on the payload.

Fundamentally, PMA’s work differently than impact attenuation devices such as airbags or paper honeycomb. Retraction mechanisms manage to decelerate the payload during the descent in order to reduce its impact velocity while, for impact attenuation devices, the impact velocity is a constraint under which the deceleration of the payload *after impact* must be reduced. This is the most significant reason why the tests described in this paper differ from the procedures to test the performance of an EFIA.

As is the case for airbags, retraction mechanisms have received more attention in terms of current research because of their multifunctional aspects. For instance, PMA’s introduce parafoil steering possibilities for increased accuracy of payload delivery, which are clearly out of the scope of this 16.62X project.

The uses of retraction mechanisms are ample in large and more sophisticated projects. PMA’s are complex mechanisms involving a pyrotechnic gas generator, braided fiber tubes and awkward triggering rods that impact the ground before the payload. They

are also much larger devices since their utility is precisely to contract from an initial state and would therefore never have the functionality of an EFIA, which is to save space. The PMA’s mentioned in this paper were as large as 1 ft in diameter and 25 ft long. Clearly, it would be useful to study simple and low-cost impact attenuation mechanisms as well.

4. Technical Approach

4.1 Experiment Plan

The flowchart in Figure 2 shows the sequence of steps necessary to assess the primary and secondary hypotheses discussed in section 2. The bold arrows indicate the path that leads to the assessment of the primary hypothesis and the thin arrows indicate the path that leads to the assessment of the secondary hypothesis. As seen in Figure 2, the successful assessment of the primary hypothesis is mostly independent of the completion of the secondary hypothesis. Similarly, the metrics that are relevant to the primary and secondary hypotheses are indicated in the flowchart. This section describes the path of the primary hypothesis first and then the path of the secondary hypothesis.

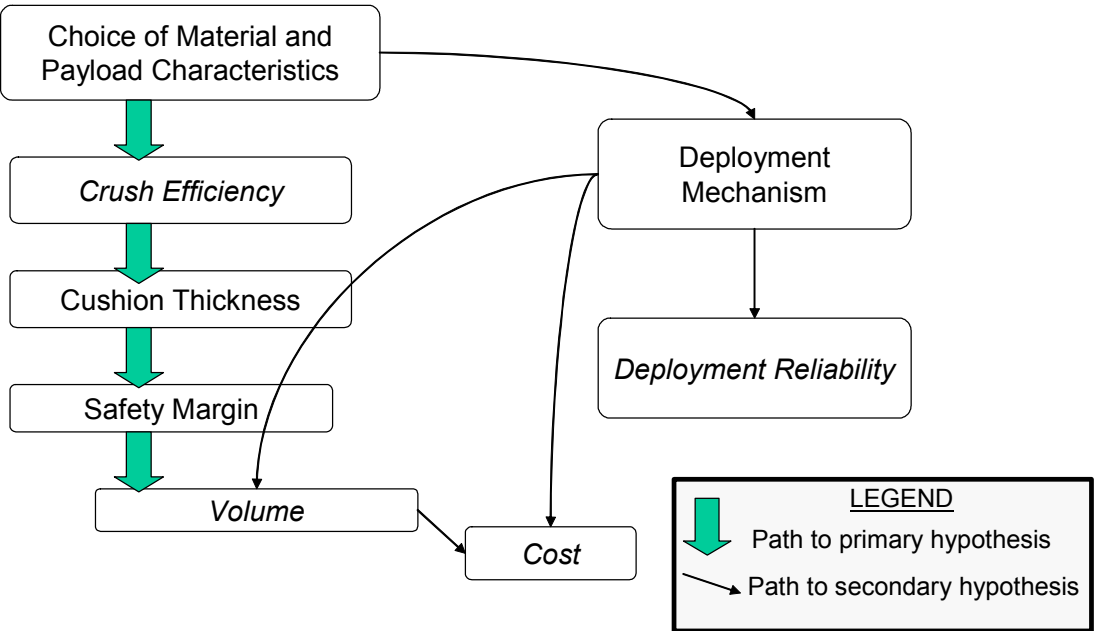


Figure 2: Experiment Plan

The initial step to take in order to perform this experiment will be to adapt an existing expanding foam product that can be attached to a payload of standard size for impact attenuation. Instapak Quick® is a market product used for packing applications in which foam expands into a rectangular bag, as shown in Figure 1. This will be adapted for

the purpose of this experiment. Paper honeycomb will be used as a baseline against which to assess the performance of expanding foam in protecting payloads delivered by small parafoils.

1. *Choice of Material and Payload Characteristics*

The appropriate base area (A_{impact}) and mass of the payload ($m_{payload}$) need to be selected simultaneously to the dynamic crush stress of the attenuation material ($\sigma_{dynamic}$). Note that, given the modeling assumption that the landing is a perfectly vertical descent, the base area of the payload will be the same area of attenuation material that impacts the ground when the payload lands. The dynamic crush stress is a property of the attenuation material, defined as

$$\sigma_{dynamic} = \frac{F}{A_{impact}} = \frac{m_{payload} Gg}{A_{impact}} \quad (\text{Eq. 1})$$

In Equation 1, g stands for the acceleration due to gravity and G is the deceleration or impact shock on the payload. A 50g-impact shock limit will be enforced, based on typical impact shock resistance values of electronic equipment. Since delicate electronic equipment is a common payload for small UAV's to deliver, this impact shock limit is consistent with the motivation of this experiment.

Since the impact shock limit is fixed, the three remaining variables that have to be chosen are the dynamic crush stress of the material, the impact area and the mass of the payload. Paper honeycomb products in the market are sold with specified dynamic crush stresses. The dynamic crush stress of foam packaging products like Instapak® can also be easily determined. Although only a discrete set of crush stress values exists for each attenuation material, both honeycomb and expanding foam products have been chosen that have a crush stress of 9 psi. This dynamic crush stress is a value that has been used previously for small payload protection with paper honeycomb. Christian Anderson advised this decision based on his experience in this field at C.S. Draper Laboratories.

The remaining parameters in Equation 1, that is the impact area and the mass of the payload, can be varied as is necessary. The impact area will be 15" x 18" because these are the dimensions of the bags into which Instapak® expands and honeycomb can easily be cut to these dimensions. Note that this baseline impact area is consistent with

typical payloads of small UAV's, which typically are about 3cu. ft. The mass of the payload should therefore be 45 lb as evaluated using Equation 1.

Note that an impact attenuation material will usually be chosen for a specific payload size and mass. Contrary to this and given the comparative aspect of this project, impact attenuation materials with similar dynamic crush stresses were the limiting factor in the calculations described above.

The chosen paper honeycomb and expanding foam products must be acquired and a nominal payload built according to the parameters described above. The crush thickness efficiency of both the honeycomb and the expanding foam can then be obtained empirically and compared.

2. Crush Thickness Efficiency

The crush thickness efficiency, as defined for the purposes of this project, is given by the ratio of the crush displacement x_{crush} of a material that is crushed completely to the initial thickness of the cushion of material ($\tau_{cushion}$).

$$\eta_t = \frac{x_{crush}}{\tau_{cushion}} \quad (\text{Eq. 2})$$

Note that a material can be assumed to have crushed completely by evaluating a plot of the displacement of the material as it is crushed versus the compressive force that is being applied. This plot resembles that which is illustrated for paper honeycomb in Figure 3.

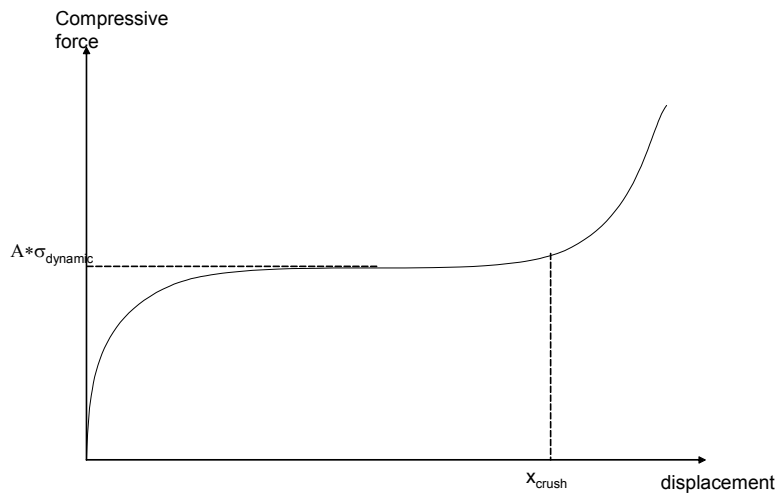


Figure 3: Plot of displacement vs. Compressive force for paper honeycomb

The material is said to be crushed completely when a considerable force will not displace the material significantly. Once this threshold in compression has been reached, the crush displacement becomes virtually independent of the force applied.

Each material will be crushed completely in a force press in order to evaluate the static crush thickness efficiency. The resultant values of crush efficiency may be confirmed with dynamic drop tests, where a minimal initial thickness of material will protect payloads of constant weight and base area that will be dropped from the same height. If the impact is strong enough for the material to crush completely, the crush displacement will be measured and the crush efficiency confirmed.

Even if the material has a damping effect (such that the force required to crush it completely is a function of the velocity with which the material is impacted), the results for the thickness efficiency of the dynamic tests should not differ significantly from the results of the static tests. This is because, as shown in Equation 2, the thickness efficiency is not a function of the force. There is also no reason to believe there will be a damping effect for either material. Therefore, the dynamic tests will be performed if the material can be impacted strongly enough at the test rig available.

The final result will be expressed as a percent difference in crush efficiency between materials as compared to the paper honeycomb crush efficiency.

3. Cushion Thickness

Having evaluated the crush thickness efficiency of the materials, one can determine the cushion thickness required to prevent the payload from experiencing a shock above 50g. From one-dimensional kinematics and the definition of crush thickness efficiency in Equation 2, the following equation for the cushion thickness is found:

$$\tau_{cushion} = \frac{v_0^2}{2gG\eta_t} \quad (\text{Eq. 3})$$

In Equation 3, v_0 stands for the impact velocity. A test rig will be built of the appropriate height such that impact velocity will be 15 ft/s. A mass falling from approximately 3.5 ft will reach this impact velocity. Therefore, the height of the test rig will exceed 3.5 ft such that the drop can be calibrated to assure a 15 ft/s impact velocity.

The nominal impact velocities of small parafoils that are currently being used for payload delivery motivate this impact velocity value.

The value of the cushion thickness that Equation 3 yields will be used in the subsequent tests to determine a safety margin on the impact shock limit of the payload.

4. *Safety Margin Tests*

For these tests, we will collect a broad sample of values of impact shock on the payload after a series of test drops using both materials. The impact shock G will be measured with an accelerometer on board of the payload. The cushion thickness used during these test drops will be the minimum necessary according to Equation 3 such that the impact shock does not exceed 50g and the safety margin ΔG will be defined as two standard deviations from the mean of the sample. The size of this sample is required to be 25 data points for each material in order to have a 95% confidence that 95% of the true population fall below 2 standard deviations from the mean of the sample. This analysis was performed by Julie Arnold and Christian Anderson and is included in Appendix C.

The safety margin will determine a final cushion thickness

$$\tau_{final_cushion} = \frac{v_0^2}{2g(G - \Delta G)\eta_t} \quad (\text{Eq. 4})$$

This final cushion thickness will be taken into account when we compare the pre-deployment volume taken up by the two attenuation materials.

5. *Pre-Deployment Volume*

This is the total volume of the impact attenuation device, including all the material needed for the effective attenuation of the nominal payload, as it will lie in the payload compartment of a UAV. Once again, the thickness of material considered will be that which will provide the final cushion thickness that the safety margin tests yield. If a deployment mechanism for the EFIA is developed, the volume taken up by any additional components involved in this mechanism will be included in the measurement. The result will be expressed as a percent decrease in the pre-deployment volume taken up by the expanding foam as compared to the paper honeycomb.

6. *Deployment Mechanism*

A mechanism should be designed to automatically deploy the expandable foam cushion while it is attached to the payload. This design will only be performed if there is enough time and resources. Otherwise, a set of functional requirements for the design of the deployment mechanism will be laid out according to the results of the rest of the experiment. The design criteria that will motivate these functional requirements will be the secondary hypothesis stated in section 2.1.

7. *Mechanical Reliability*

The initial assumption for this metric is that the reliability of paper honeycomb is 100% because honeycomb does not rely on any mechanism to be deployed. A number of Instapak bags will then be deployed, and the number of trials with successful foam expansion within 2 minutes will be recorded. Note that a trial will be considered successful only if the foam expands to the prescribed thickness and in the prescribed time lapse as stated by Instapak® manufacturers. The criteria for this definition of reliability will therefore be that the desired impact attenuation is provided and that the foam in a UAV payload would expand before touchdown.

The mechanical reliability of the expanding foam impact attenuation device will then be evaluated as the ratio of successful trials to the sample size. The result will be expressed as the percent loss in the mechanical reliability of expanding foam as compared to that of paper honeycomb.

8. *Cost*

This will be expressed as the percent difference in the current market price of the expanding foam as compared to that of the paper honeycomb. In each case, the cost considered will be that of the total amount of material needed to satisfy the same nominal requirements, plus an estimate of the cost of the deployment mechanism of the EFIA device if this is in fact developed. However, there are a complex set of other variables that will affect the final cost of an EFIA device and that will not be included in this tentative comparison.

4.2 Apparatus

The apparatus required to perform these tests include an Instron® force press (found at the MIT Telac laboratories) for the static crush thickness efficiency tests, and a test rig to

perform drop tests for the dynamic crush thickness efficiency tests and to find the distribution of impact shock on the payload, from which a safety margin is determined.

The instrumentation required to collect all measurements include:

- A ruler to measure the pre-deployment volume of paper honeycomb;
- A beaker to measure the pre-deployment volume of the EFIA device accurately;
- An accelerometer to measure the impact shock during the safety margin tests;
- A high speed camera to record the displacement of the crushed materials during the dynamic crush thickness efficiency tests;
- A digital timer with photo-gates to confirm the impact velocity of the payload;
- Two computers to input the data acquired from the aforementioned instrumentation; and
- The force press, which outputs load and displacement during the static crush thickness efficiency tests.

The test rig will consist of two rails that will guide the payload in a vertical descent and that will be held up by two Unistrut® frames. These frames plus a beam holding a pulley (from which the payload will hang) will be attached to the strong wall at the MIT Aeronautics and Astronautics Department. The wire rope holding the payload will be attached to a quick-release loop and to a winch.

The main functions of the rails are to guide the payload in a vertical descent and to ensure that the bottom surface of the payload lands horizontally, such that the impact attenuation material is crushed evenly upon impact. The pulley and the quick-release mechanism are necessary such that the payload can be released from a distance and the falling weights do not constitute a hazard. The winch will be helpful to lift the payload before every drop during the tests. Finally, it should be noted that only the beam that holds the pulley will support the weight of the payload and that it will be securely clamped to the strong wall. The frames holding the rails will also be clamped to the strong wall such that the rails are secured in their position.

Detailed sketches of the test-rig configuration are included in Appendix A and considerations about the setup of the test rig are included in section 6.1.

4.3 Test Articles

The test articles will be:

- Both impact attenuation materials;
- The payload box, to which the impact attenuation materials will be attached during the drop tests; and
- The EFIA deployment mechanism that will be tested for mechanical reliability.

The impact attenuation materials will be attached to the payload with duct tape. Although this may not be ideal during the descent of the parafoil, it is the most practical configuration for performing multiple tests using the same payload. Figures 4(a) and (b) show the two impact attenuation materials: paper honeycomb, produced by Pactiv(TM); and Instapak®, the type of expanding foam that will be used for this project.

The payload will consist of a plywood box, as shown in Figure 5, with the base area and space to fit weights as discussed in section 4.1. The weights will be bolted down to the payload box to prevent any safety hazards and the effects that the rebound of the weights might have on the impact shock measurements. The payload will also be adapted so that

- The payload can be attached to the linear bearings that will slide along the rails of the test rig,
- The accelerometer can be mounted towards the base of the payload (in order to minimize vibration after impact); and
- The blinder that intercepts the photo-gates at impact can be mounted in the appropriate position.

Holes should be drilled on the upper edges of the payload box so that this can be tied to the rope wire that will feed into the pulley.

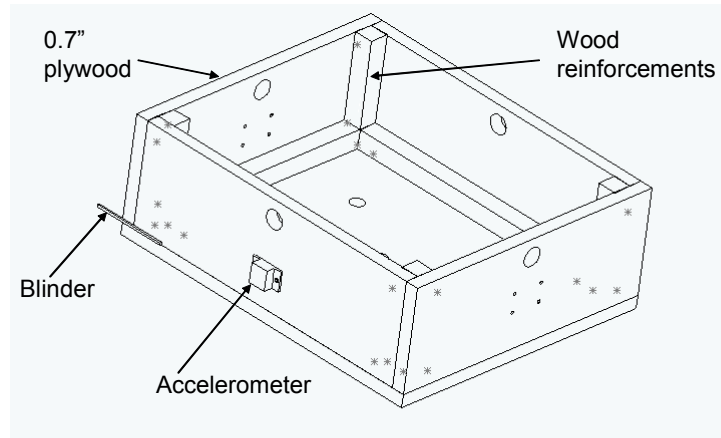


Figure 5: Payload Box Isometric View

Detailed drawings of the payload are included in Appendix A and considerations about its construction are included in section 6.2.

4.4 Test Matrices

4.4.1 Crush Thickness Efficiency Tests

The parameter under which both crush thickness efficiency tests will be performed is the initial thickness of the cushion, which, as described in section 4.1, will be the smallest thickness possible. The dependent variable is the material since the test will be performed for both honeycomb and expanding foam. The independent variable of the test is the crush displacement, from which the crush thickness efficiency will be calculated according to Equation 2. These variables are shown in Table 1. Four such matrices will exist: one for each material in both the dynamic and the static tests.

Table 1: Test Matrix for Each Material in Crush Thickness Efficiency Tests

Trial number	Initial Cushion Thickness τ (in)	Crush Displacement x_{crush} (in)	Crush Thickness Efficiency η_{crush}
1-5			
		Average	

4.4.2 Safety Margin Tests

The parameters for the safety margin tests will be an impact velocity of 15 ft/s and the cushion thickness required of each material according to Equation 3. The independent variable is once again the material, such that the test matrix shown in Table 2 will be used both for honeycomb tests and for EFIA material tests. The test will be performed for a number of trials, and the dependent variable that will result from each of these trials is the maximum impact shock G on the payload.

The safety margin ΔG will be twice the size of the standard deviation of the distribution obtained from these trials.

Table 2: Test Matrix for each Impact Attenuation Material in Safety Tests

Trial Number	Maximum Shock Recorded G (ft/s²)
1-25	

4.4.3 Pre-Deployment Volume Measurements

In the pre-deployment volume measurements, the independent variable is the attenuation material/device and the dependent variable is the volume measured.

These variables are shown in Table 3.

Table 3: Test Matrix for Pre-deployment Measurements

Impact Attenuation	Pre-Deployment Volume (ft³)
Paper Honeycomb	
EFIA device	

4.4.4 Mechanical Reliability Tests

The mechanical reliability will be measured only for the deployment mechanism of the EFIA device. The parameters that will be assessed are the final cushion thickness that the material is expected to expand to and the time expansion is expected to take. The test will be performed for a number of trials and the dependent variables that will result will be the cushion thickness of the expanded material and the time for full expansion. These values will yield a yes or no answer to whether the expansion was as expected, from which a final value of the mechanical reliability will be determined as explained in section 4.1.

Table 4: Test Matrix for Mechanical Reliability Tests

Trial Number	Time to Expand (seconds)	Final Cushion Thickness τ (in)	Appropriate Deployment (Y/N)

5. Discussion of Errors

All uncertainties that are identified in this section are stated in Section 7.3, which includes a discussion of how these uncertainties are propagated to the metrics that will be evaluated from direct measurements.

5.1 Crush Thickness Efficiency

In order to achieve the success criteria proposed in section 2.3, the accuracy to which values of crush thickness efficiency and pre-deployment volume are determined must be known. As Equation 2 suggests, the random errors involved in evaluating the crush thickness efficiency can be traced back to the errors involved in measuring and determining the initial cushion thickness and the crush displacement. The error in the initial cushion thickness is the accuracy of the ruler that will be used to measure it. The error in the crush displacement is slightly more complicated.

As discussed above, the crush displacement for a material that is crushed completely can be obtained from displacement versus compressive force plots. The end of the plateau illustrated in Figure 3, which marks the crush displacement, may be hard to determine from these plots. In order to reduce this inaccuracy, the tests will be performed 5

times for each material and the final value of crush thickness efficiency will be the average of the sample.

It should be noted that these plots will be derived from force (or deceleration) and displacement measurements at the force press or at the test rig. The force press will output these values directly, while at the test rig the deceleration or impact shock will be measured with the accelerometer and the crush displacement will be measured with the high speed camera.

5.2 Pre-Deployment Volume

The random error in the pre-deployment volume measurements is the accuracy of the instruments used to measure volume, that is, the accuracy of ruler used to measure the volume of the paper honeycomb and the accuracy of the beaker used to measure the volume of the pre-deployed expanding foam.

However, the pre-deployment volume depends directly on the final cushion thickness, which takes into account the safety margin.

5.3 Safety Margin Tests

The final cushion thickness will be evaluated using Equation 4 and will include a bias error due to the inaccuracy of two parameters that are experimentally determined. The first is the crush thickness efficiency, determined during the crush thickness efficiency tests. The second is the calibration of the test rig to enforce an impact velocity of 15ft/s. This calibration is limited by the accuracy of the digital timer and the photo-gates that will be used to measure impact velocity.

The other parameter that is experimentally determined and that will affect the final cushion thickness is the safety margin, ΔG . Since the safety margin tests are done providing a marginal or initial cushion thickness, there will be a bias error in the distribution of impact shock that is observed. This bias error will also emerge from, similarly to what is discussed above, the crush thickness efficiency and the calibration of the test rig to the appropriate impact velocity.

Finally, the random error involved in the measurement of each shock and that will affect the safety margin is the accuracy of the accelerometer, combined with the ability to release the payload from the same height after each test.

5.4 Additional Considerations

There is an important measurement system implied in the recording of the highest impact shock on the payload during the safety margin tests. The accelerometer will be analog, but the accelerometer reading is sampled into a computer discretely, such that the highest impact shock value could be lost.

The time lapse for the attenuation material crush can be calculated with one-dimensional kinematics for a deceleration from 15 to zero ft/s given an impact shock (deceleration) of 50g. This lapse is of the order of 0.01 s. In order to have an accurate curve of the impact shock on the payload during this lapse of time, a sampling frequency of at least $5/0.01$ s, that is, 500 Hz is required². The data acquisition computer that will be used has a sampling frequency of 100 kHz and it samples data from the accelerometer through 3 different channels (corresponding to three orthogonal axes), resulting in a sampling rate in the vertical direction of more than 30 kHz. This means that there is no considerable risk that the impact shock signal from the accelerometer will be damped.

Of the uncontrolled inputs to our tests, human and machine errors are included in the instrument accuracy values. Other uncontrolled inputs will be mostly ambient changes, in particular affecting the expansion of the EFIA material. This error will be taken into account within the safety margin that will be determined.

6. Construction Procedures

Please refer to Appendix A for detailed drawings of the drop test rig and the payload box that will be constructed. All materials and instrumentation that this section refers to are listed in detail in Appendix B.

6.1 Drop Test Rig

1. The Unistrut lengths that will be used to build the frames of the test rig and to hold the pulley must be cut to the appropriate length at the machine shop of the MIT Department of Aeronautics and Astronautics. This includes:
 - 2 front beams that are 24.58" long,
 - 4 side beams that are 18.65" long, and
 - 1 cantilever beam that is 13.125" long.

Unistrut beams are shown in Figure 6:

2. Two holes will be drilled in each of the 18.65" long pieces of Unistrut, where the shaft supports will be bolted to the frame. These holes will have a diameter of 0.11" and will be located on the face of the Unistrut opposite to the channel, centered along the length of the beam, 1.5" apart and 0.85" from the side of the beam.
3. The top and bottom Unistrut frames will be assembled with right angled fittings running along the outer side of the frame, as sketched below:

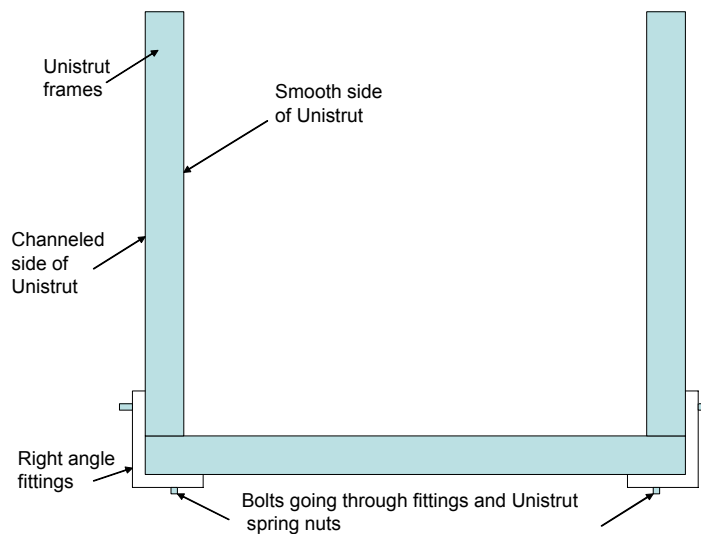


Figure 7: Top view of frame assembly

4. The pulley will be attached 10.125" from one end of the cantilever beam.
5. The assembled frames will be clamped with I-beams to the strong wall, one at the level of the floor and the other at a height of 6 feet. The cantilever beam holding the pulley will be clamped with an I-beam, 7 feet above the ground and between the sides of the upper frame.

6. Two ball bearings will be inserted in each shaft and then a shaft support will be tightened at both ends of the shaft.
7. The shaft supports will be bolted to the holes on the sides of the frames. The interface between the Unistrut beam, the shaft support, the shaft and the ball bearings that will be bolted to the payload is sketched in Figure 8. Detailed drawings of this interface are also included in Appendix A.

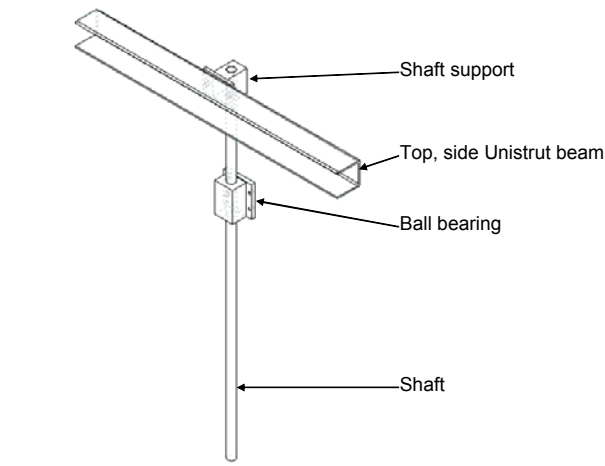


Figure 8: Test Rig Detail Isometric View

6.2 Payload Box

1. The blinder that intercepts the photo-gates has to be milled at the machine shop. It must be 4" long and 0.120" +/- 0.005" wide.
2. All sides of the payload box and the inner reinforcements have to be sawed to the appropriate dimensions, as specified in Appendix A.
3. Holes must be drilled on the faces of the payload box as follows:
 - 4 holes on each side face to attach to the ball bearings on the shafts.
 - A hole towards the top of each face from which the payload will be tied to the rope wire.
 - 2 holes on the front face to attach the accelerometer to the payload.
 - 5 holes on the bottom face to insert bolts that will hold the weights inside the payload in place.

The diameters and locations of all holes are specified in Appendix A.

4. The box will be held together with wood screws and reinforced with 1” by 1” wood blocks running along every inner edge. The locations of these screws are specified in Appendix A.
5. The bolts for the accelerometer and the weights will be attached in their appropriate location. Note that the accelerometer should be placed such that the connecting wires will be plugged in at the top. This way the wires will not hit the frame nor get entangled between it and the payload during the fall.
6. The photo-gate blinder will be glued with industrial adhesive to the bottom of the front face of the payload box, protruding to one side as sketched in Appendix A.
7. The payload will be weighed to determine what additional load needs to be added.

6.3 Set-up

1. A metal L will be clamped to the side of the bottom frame in the location specified in Appendix A. The photo-gate will be stuck with duct tape to this metal L such that it can be relocated for different drop tests in which the thickness of the attenuation material will change. The height at which the photo-gate must be held before each test will be such that the blinder on the payload lies just below the photo-gate when the payload is laid on the platform.
2. A 2” by 15” by 18” wood platform will be placed on the floor inside the bottom frame of the test-rig such that the impact is even.
3. The payload box will be attached to the ball bearings on the shafts.
4. Weights as needed will be put through the bolts on the base of the payload and trying to distribute the load evenly across the area.
5. The payload will be tied with rope wire, which will be fed through the pulley and connected to the quick release off the floor of the strong wall. The winch will also stand at this location to pull the payload up before each drop.
6. The high speed camera will be placed 2” above the floor besides the test rig and opposite to the location of the photo-gate such that connecting wires don’t conflict. Note that the camera will be aimed at the top of the platform where impact will occur.

7. A ruler will be placed vertically next to the platform and facing the high speed camera.

6.4 Safety concerns

During the construction of the test-rig and during the tests at the test-rig site and at Telac, a conservative attitude will be maintained. Julie Arnold has attended the machine shop training session and she will be in charge of milling the Unistrut beams and the photo-gate blinder while observing all safety procedures. Tests will be performed at the force-press under John Kane's guidance.

The test-rig has been designed such that the payload can be released from a few meters apart to prevent accidents due to the falling load. Furthermore, the weights will be bolted down in the payload such that they don't fall off during the fall.

Both Julie Arnold and I will be present at all construction and data-collection sessions, to assist each other if necessary.

7. Data Acquisition and Analysis

7.1 Measurement Systems

At the test-rig, data will be acquired separately from the accelerometer, the high-speed camera and the digital timer. The accelerometer outputs to a stand-alone analog to digital board through a five pin connector. One of the pins has to be connected directly to a 5 volt battery, another pin is grounded and other three pins output voltages corresponding to the induced acceleration in three axis. This A/D board inputs the data to a computer for later reduction using National Instrument's LabVIEW software. This data may then be transferred to Matlab in order to draw displacements versus force plots with the data collected from the high-speed camera.

The high-speed camera is connected to a separate computer and has its own software. The software records still frames at 8000Hz and, after it is calibrated with the ruler seen on the image, it will read off the distance between two points where the cursor is set. Namely, it will provide the displacement of the crushed material.

The photo-gates are connected directly to a stand-alone digital timer from which the impact velocity of each trial can be read off. This will be useful before the tests to calibrate the height from which the payload must be released such that the impact velocity is as close to 15ft/s as possible.

At Telac, the force press outputs load, displacement and time directly to a computer. The data can be viewed in any data analysis software.

7.2 Data Reduction

7.2.1 Static Crush Thickness Efficiency Tests

Two sets of data will be obtained from these tests: the initial thickness of each sample of impact attenuation material and the displacement versus compressive force plots from the computer connected to the force press. Two results will be derived from this data:

- The average force values that lie on the plateau of these plots will be averaged. This average value can be divided by the payload base area to confirm the dynamic crush stress of each material, as shown in Figure 3.
- For each attenuation material, the crush displacement will be extracted from each plot and divided by the initial cushion thickness to give the crush thickness efficiency of each sample. These values will then be averaged for each impact attenuation material.

7.2.2 Dynamic Crush Thickness Efficiency Tests

The data obtained from these tests will be the initial thickness of each sample, the picture frames from the high speed camera and the impact shock versus time plots from the computer that is connected to the accelerometer. The crush displacement of a set of frames will be extracted using the software that accompanies the high-speed camera. These displacement values will be plotted against the impact shock values obtained from the accelerometer using Matlab. If a plateau is observed in these plots, a crush displacement value will be extracted. The crush thickness efficiency of each test will then be evaluated and an average value will be found for both paper honeycomb and expanding foam.

The data will be analyzed such that, if the impact attenuation material does not crush completely, the static crush thickness efficiency will be used in subsequent tests. With the chosen crush thickness efficiency value, the marginal crush thickness necessary for the safety margin tests will be evaluated using Equation 3.

7.2.3 Safety Margin Tests

The data obtained from these tests are the impact shock versus time plots from the computer connected to the accelerometer. The maximum impact shock value of each of these tests must be extracted and put into Matlab. From Matlab, the sample distribution, its mean and the value of two standard deviations will be extracted.

Subsequently, the final cushion thickness will be evaluated using Equation 4. The final cushion thickness will be multiplied by the payload base area in order to find the pre-deployment volume of the paper honeycomb.

Since the pre-deployed expanding foam comes in discrete volume increments (the volume of each pre-deployed Instapak bag), the number of pre-deployed bags necessary to reach or exceed the final cushion thickness will be evaluated.

7.2.4 Pre-Deployment Volume of EFIA

The number of Instapak bags determined to satisfy the final cushion thickness after the safety margin tests will be submerged in a beaker. The volume of water displaced will be the pre-deployment volume of the EFIA.

7.2.5 Deployment Reliability Tests

The data collection for this test will run parallel to all other tests: each time an Instapak bag is deployed, the time it takes to fully expand and the thickness of the expanded cushion will be recorded. This data will be entered in Table 4 and a correct deployment will be assessed. The number of successful deployments will be divided by the number of samples to obtain the reliability of the Instapak mechanism.

7.2.6 Hypothesis Assessment

The values of crush thickness efficiency, pre-deployment volume and deployment reliability of the EFIA will be expressed as a percent of the respective values of paper honeycomb. These results will be presented in bar graphs as shown in Figure 9.

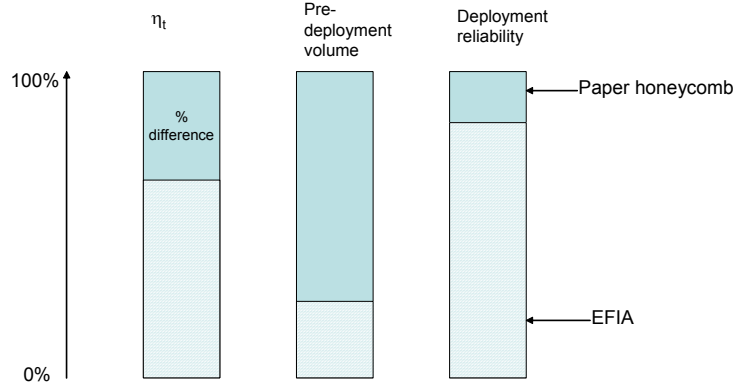


Figure 9: Hypothesis Assessment Bar Graphs

7.3 Error Analysis

The accuracies of the instrumentation used for this project are:

- Ruler accuracy: 0.0625”
- Force press displacement accuracy: 0.01”
- High-speed camera sampling rate is 8kHz, therefore the time between frames is 1.25×10^{-4} seconds
- Crossbow accelerometer series CXL100HF3
 - range: -100g to 100g
 - accuracy due to sensitivity: 2%
 - accuracy in measurements around 50g: 1g
- Photo-gate samples light at 1 MHz, therefore time measurement accuracy: 10^{-6} seconds

Note that all independent errors that affect a certain metric will be combined according to the general rule for combination of errors:

$$dz = \sqrt{\left(\frac{\partial F}{\partial x_1}\right)^2 dx_1^2 + \left(\frac{\partial F}{\partial x_2}\right)^2 dx_2^2 + \left(\frac{\partial F}{\partial x_3}\right)^2 dx_3^2 \dots} \quad (\text{Eq. 5})$$

In Equation 5, $z = F(x_1, x_2, x_3 \dots)$.

7.3.1 Crush Thickness Efficiency Measurement Errors

Static Tests

The measurement error in the crush thickness efficiency is due to the accuracy of the force press and the ruler. From Christian Anderson’s experience with paper honeycomb, it is known that a typical initial cushion thickness would be

2”, which will crush about 1.3”. The crush thickness efficiency of paper honeycomb is known to be about 63%. Based on this data the general rule for combination of errors can be applied to Equation 2 as follows:

$$d\eta_t = \eta_t \sqrt{\left(\frac{dx_{crush}}{x_{crush}}\right)^2 + \left(\frac{d\tau_{cushion}}{\tau_{cushion}}\right)^2} \quad (\text{Eq. 6})$$

The static crush thickness efficiency tests will therefore be accurate to 2.1%, which is acceptable to achieve the success criteria stated in section 2.3.

Dynamic Tests

The error in the measurement of crush displacement during the dynamic tests is affected by two sources of error, namely the sampling frequency of the high-speed camera and the accuracy of the ruler that is used to scale the picture frames.

The error due to the sampling frequency of the camera can be conservatively quantified by assuming that, in a perfectly elastic collision, two consecutive frames are frozen 6.25×10^{-5} seconds (half the time between frames) before and after the maximum displacement. Assuming an acceleration of 50g, this scenario would result in an error in the crush displacement measurement of 3.78×10^{-5} inches. The combined error due to the accuracy of the ruler and the sampling rate would therefore be 0.063”. This result shows that the error due to the sampling of the camera has a negligible effect on the combined error of the crush displacement.

The combined error in crush displacement can itself be combined, as was done for the static tests, with the error of the initial cushion thickness measurement, leading to a measurement error of 3.75% in the dynamic crush thickness efficiency values.

Note that, if dynamic crush thickness efficiency values are indeed found experimentally, these –rather than those resulting from static tests- will be used to determine other parameters in subsequent tests. For this reason, the error analysis that follows takes into account a possible error of 3.75% in crush thickness efficiency values.

7.3.2 Pre-Deployment Volume Measurement Errors

The pre-deployment volume of paper honeycomb will be determined by the accuracy of the ruler that will be used to measure the width, depth and height of the

honeycomb sample. Assuming a base area of 15” x 18” and a final cushion thickness of 2.5”, the possible error will be 11% of the volume of the honeycomb sample.

The accuracy of the beaker that is used to measure the volume of Instapak bags must be such that the pre-deployment volume of expanding foam is shown to be at least 86% less and at most 66% less than the volume of paper honeycomb. This will allow the fulfillment of the success criteria.

7.3.3 Final Cushion Thickness Errors

Bias Error Effects on the Maximum Impact Shock Distribution

As mentioned in section 5, the final cushion thickness will be affected by both bias and random errors when a safety margin is determined.

The bias error in the distribution of maximum impact shock values will be due to the inaccuracy of the specifications used to set up the tests, which are also experimental results. As can be seen from Equation 3, the actual impact shock felt by the payload will be a function of the marginal cushion thickness, the impact velocity and the crush thickness efficiency. The impact velocity will be biased because of inaccurate calibration of the test rig, whether because of the inaccuracy of the digital timer reading or the inability to release the payload from the precise height from which it would impact at 15ft/s. The crush thickness efficiency is the direct result of previous tests, as discussed in section 7.3.2. The marginal cushion thickness will be evaluated using that same result.

The accuracy of the impact velocity measurements is determined by two different sources of error. The digital timer provides virtually instantaneous velocity measurements by dividing the width of the photo-gate blinder by the time during which the blinder intercepts the photo-gate light beam. The sources of error in this measurement are therefore the sampling rate of the photo-gate and the fact that the photo-gate blinder accelerates while intercepting the light beam.

The error dv_1 due to the sampling rate is the combined accuracy of the digital timer and the accuracy $dw_{blinder}$ to which the width of the blinder is milled:

$$dv_1 = v \sqrt{\left(\frac{dw_{blinder}}{dw_{blinder}}\right)^2 + \left(\frac{dt_{sample}}{t_{sample}}\right)^2} \quad (\text{Eq. 7})$$

The error dv_2 due to the acceleration of the blinder can be at most one half of the change in velocity that the blinder undergoes while intercepting the photo-gates:

$$dv_2 = \frac{1}{2} \sqrt{2g w_{blinder}} \quad (\text{Eq. 8})$$

The combined velocity error can then be found using Equation 5, which yields an uncertainty of 0.743ft/s or 0.05% of an impact velocity of 15ft/s.

Since the error in the dynamic crush thickness efficiency value is known, the error in the marginal or initial cushion thickness can be evaluated using Equation 3 as follows:

$$d\tau_{cushion} = \sqrt{\left(\frac{v_0^2}{2gG\eta_i^2}\right)^2 d\eta_i^2} \quad (\text{Eq. 9})$$

The specifications to determine the initial cushion thickness will be: an impact shock of 50g, an impact velocity of 15ft/s and the crush thickness efficiency value that results from dynamic tests (assumed for this calculation to be 63%). The resulting uncertainty in the marginal cushion thickness evaluation is thus 0.234”.

All the errors mentioned above can be assumed random and independent. The combined bias error that will shift the mean of the maximum impact shock distribution can thus be calculated using Equation 5, which yields a possible shift of 10.9g’s from the true mean.

Random Error Effects on the Maximum Impact Shock Distribution

The two random error effects on the impact shock are due to the accuracy of the accelerometer and the height to which the payload is set before the drop. The payload will be set to a mark on the shafts of the test-rig to an accuracy of about 0.125”. The impact velocity achieved will therefore be 15 +/- 0.819ft/s. Assuming a crush thickness efficiency of 65% and a cushion thickness of 2” are specified, Equation 3 yields an impact shock of 50 +/- 5.34g.

Combining the uncertainty due to instrumentation accuracy and the height the payload is set to, the uncertainty of the impact shock will be 5.43g. This random error means that maximum impact shock values that are within 5.34g of the

mean of the distribution can not be attributed to variations in the impact attenuation material, which is what the safety margin aims to account for.

Final Cushion Thickness Error

Since the error in the dynamic crush thickness efficiency value and the random error in the impact shock are known, the error in the final cushion thickness can be evaluated using Equations 4 and 5 as follows:

$$d\tau_{final_cushion} = \sqrt{\left(\frac{v_0^2}{2g\eta_t(\Delta G - G)}\right)^2 d(\Delta G)^2 + \left(\frac{v_0^2}{2g\eta_t^2(\Delta G - G)}\right)^2 d\eta_t^2} \quad (\text{Eq. 9})$$

The specifications to determine the final cushion thickness will be: an impact shock of 50g, an impact velocity of 15ft/s and the crush thickness efficiency value that results from dynamic tests (assumed for this calculation to be 63%). The resulting uncertainty in the final cushion thickness evaluation is thus 0.3". Note that the bias errors are not included in this calculation because they will not affect the standard deviation of the sample and therefore won't affect the safety margin determined.

8. Project Planning

This project will be completed in the fall of 2003 during 16.622. The following section includes the schedule for the completion of the project and the facilities and staff support that will be needed. Please note that the parts list in Appendix B includes details as to buy/borrow decisions, specifications for parts that must be purchased and the details of a \$560.00 budget that is estimated.

8.1 16.622 Schedule

Table 5 shows a detailed schedule for the fall term of 2003 that should ensure the timely completion of this project. The weeks in which the major milestones of 16.622 are due are also included. Note that the last two weeks to collect data will be allotted to the development and testing of the deployment mechanism for an EFIA that will allow the assessment of the secondary hypothesis as discussed in section 2.1. This includes data reduction of the deployment reliability tests that will run parallel to other tests. If a deployment mechanism is not designed, work will be done to specify the functional requirements of an eventual design.

Table 5: 16.622 Schedule

	September			October			November			December				
Week	1	2	3	4	5	6	7	8	9	10	11	12	13	14
(week starts)	8/9/2003	15/9/2003	22/9/2003	29/9/2003	6/10/2003	13/10/2003	20/10/2003	27/10/2003	3/11/2003	10/11/2003	17/11/2003	24/11/2003	1/12/2003	8/12/2003
Team meetings	☆						☆							
Oral Progress report				☆										
Final Oral Report												☆		
LAST DAY TO COLLECT DATA										☆				
Outline due											☆			
Report Due														☆
Familiarize with LabVIEW and high-speed camera software														
Gather materials and instrumentation														
Assemble test-rig and instrumentation														
Connect instrumentation and check software														
Static Crush Thickness Efficiency tests														
Dynamic crush thickness efficiency tests														
Date reduction for marginal cushion thickness														
Safety margin tests														
Safety margin data reduction														
Volume measurements														
Work on secondary hypothesis														
Prepare outline for report														
Write report														

8.2 Facilities and Staff Support

- The Department of Aeronautics and Astronautics machine shop and the help and guidance of Donald Weiner
- The strong wall at the Department of Aeronautics and Astronautics and the help of Richard Perdichizzi to gather instrumentation and materials
- The Instron force press at the MIT Telac laboratories and the guidance of John Kane

9. Summary

This project will assess whether expanding foam can be a low-cost alternative for impact attenuation of payloads delivered by small aircraft, as it minimizes pre-deployment volume as compared to paper honeycomb. The crush thickness efficiency tests will help establish whether the expanding foam used in Instapak products can provide appropriate impact attenuation as paper honeycomb has been shown to do. The safety margin tests are necessary to have a high level of confidence that the prescribed cushion thickness of impact attenuation material will protect a payload of specific characteristics. It is taking into account this safety margin that a comparison of the pre-deployment volume of the two impact attenuation materials will be done. These tests cater to the primary success criteria of the project.

An attempt will be done to satisfy the secondary success criteria. This success depends on the completed design of a way to implement expanding foam to a very specific situation. If this design is not completed, detail functional requirements will be determined. The deployment reliability tests will aid the fulfillment of this goal.

The successful completion of this project can be ascribed to thanks to the enthusiastic support of the 16.62X technical staff, the guidance of the 16.62X faculty, and Christian Anderson's unconditional encouragement.

10. References

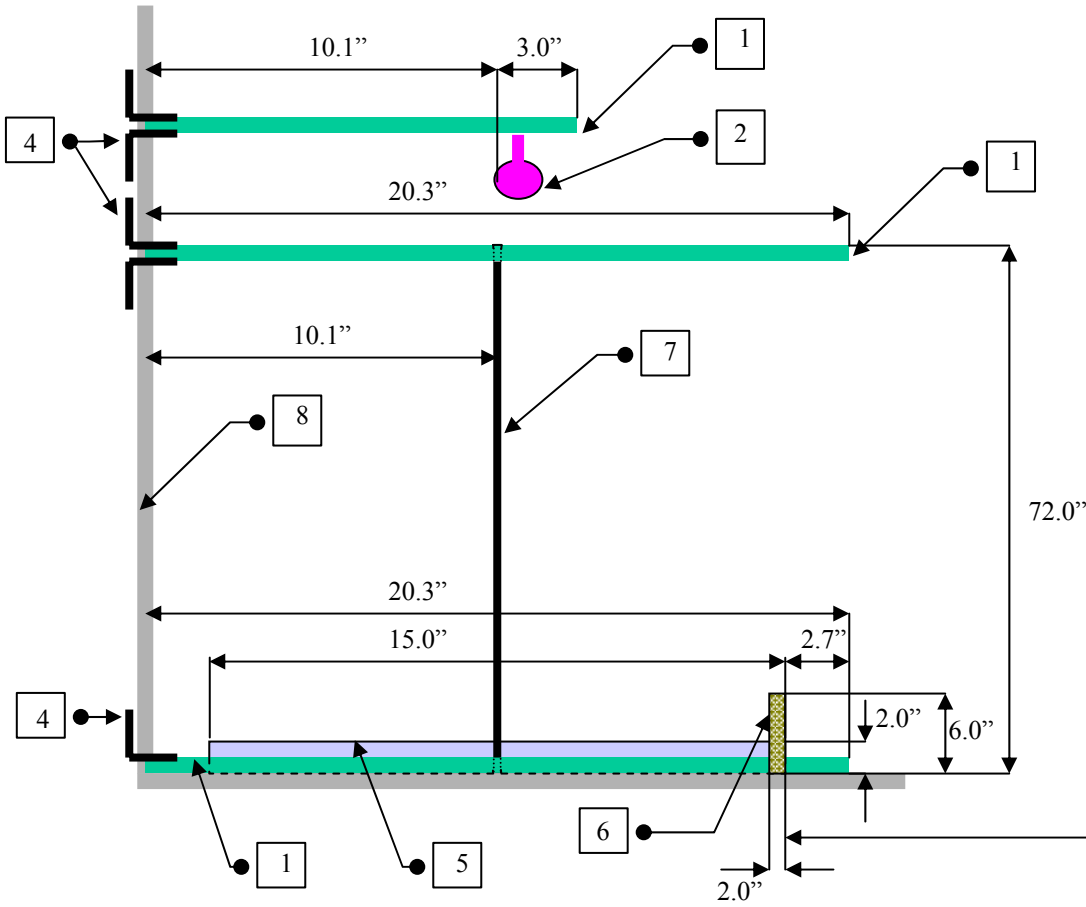
- ¹ “Cellular Plastics”, *Handbook of Industrial Materials*, 2nd ed., Elsevier Advanced Technology, Oxford UK, 1992, pp. 540-545
- ² Brown, R.P, “Instrumented Tests”, *Handbook of Plastics Test Methods*, 3rd ed., Longman Scientific and Technical, New York, Wiley, 1998, pp. 160-161
- ³ Gardinier, Yanagihara, Kobayashi, Amito, “Design and Testing of the HOPE-X HSFD-II Landing System”, *AIAA Journal*, Vol. 20, No. 48, 2001, pp. 304-310
- ⁴ G. Brown, R. Haggard, R. Benney , “Parachute Retraction Soft Landing Systems Using Pneumatic Muscle Actuators”, *AIAA Journal*, Vol. 43, No. 8, 2000, pp. 1-9

Appendix A: Detailed Drawings

The following drawings are attached:

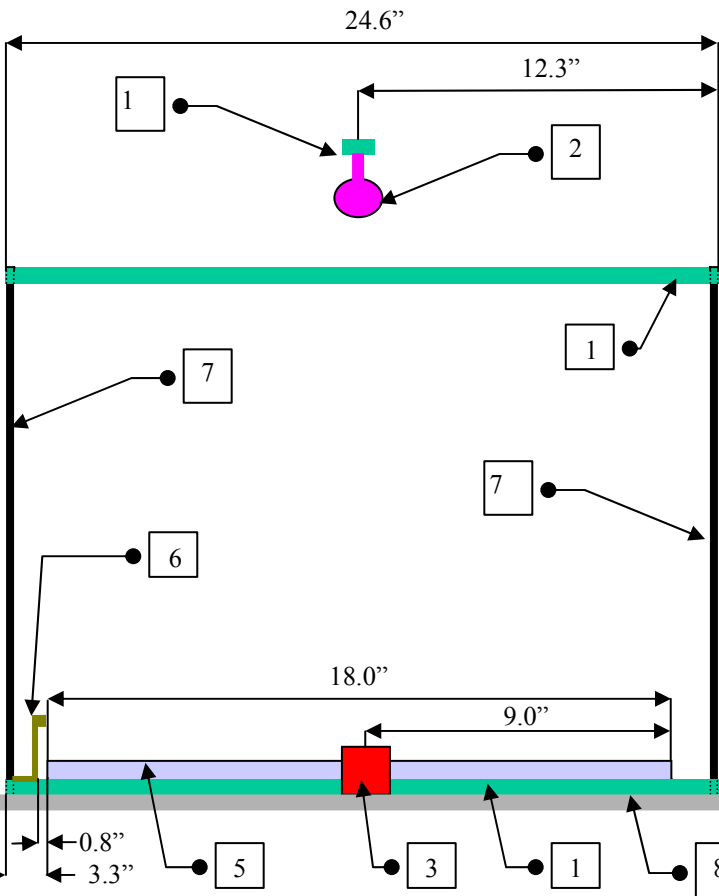
- Dimensioned, three-view drawing of drop test rig (not to scale)
- Dimensioned, four-view drawing of drop test rig detail: shaft interfaces with ball bearing, shaft support and top side of Unistrut frame
- Detail- shaft interfaces side view
- Dimensioned, three-view drawing of payload box
- Detail- payload box front view

Drop-Test Rig: Front View

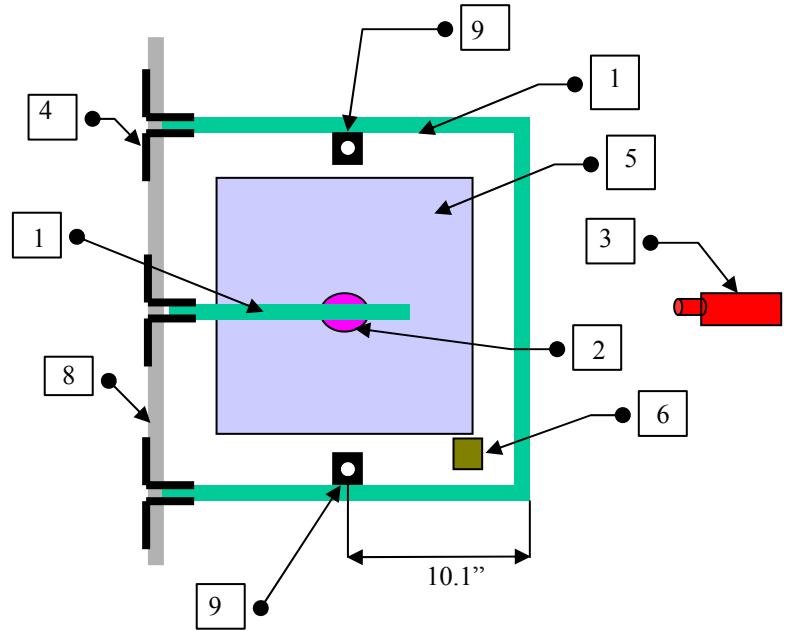


- Legend:**
- 1- Unistrut
 - 2- Pulley
 - 3- High Speed Camera
 - 4- I-Beam to Connect Unistrut to strong wall
 - 5- Wood Platform
 - 6- L-Support with Photogate
 - 7- Rail shafts
 - 8- Strong wall
 - 9- Linear Bearings
- DRAWINGS ARE NOT TO SCALE

Side View



Top View



Appendix B: Parts List, Purchase Specifications and Budget

Borrowed Parts, Tools and Materials			quantity	borrowed from
Winch			1	Richard Perdichizzi
Pulley			1	Richard Perdichizzi
Quick release			1	Richard Perdichizzi
Rope wire			30 ft	Richard Perdichizzi
McMaster shaft supports			4	Dept. of AeroAstro
McMaster Ball Bearings			4	Dept. of AeroAstro
2lb and 5lb Weights			45 lb	Dept. of AeroAstro
21" by 48" by 0.7" plywood			1 board	
Saw			1	Dept. of AeroAstro
Drill			1	Dept. of AeroAstro
Hammer			1	Dept. of AeroAstro
0.25" thick aluminum sheet for blinder			1	
Metal L to mount photo-gates			1	Dept. of AeroAstro
Duct tape			2 rolls	
Industrial adhesive			1	Dept. of AeroAstro
Screws for shaft supports			8	Dept. of AeroAstro
Screws for ball bearings			8	Dept. of AeroAstro
Screws to bolt weights			5	Dept. of AeroAstro
1 1/2" long Wood screws			20	Dept. of AeroAstro
1/2" thick Paper Honeycomb (Hexacomb 700 from Pactiv Corporation)			4 sheets 96" by 48"	
1" thick Paper Honeycomb (Hexacomb 700 from Pactiv Corporation)			8 sheets 96" by 48"	
Unistrut Metal Framing® components				
Unistrut channelled sections with smooth faces		front of frames	2 beams >= 25"	Dept. of AeroAstro
		sides of frames	4 beams >= 19"	
		cantilever beam	1 beams >= 14"	
Spring nuts			8	Dept. of AeroAstro
Fittings			4	Dept. of AeroAstro
I-beams			5	Dept. of AeroAstro
Borrowed Instrumentation				
Accelerometer			1	Christian Anderson
High-Speed camera			1	Dept. of AeroAstro
Photo-gates and digital timer			1 set	Dept. of AeroAstro
Analog to Digital board for accelerometer			1	Dept. of AeroAstro
Computers for data acquisition			2	Dept. of AeroAstro
Ruler			1	

PURCHASE SPECIFICATIONS AND BUDGET

Parts, Materials and Instrumentation to be Purchased	quantity	purchase specifications	price	suppliers
72" long, 1/2" diameter shafts for rails	2	McMaster Carr Catalog Number 6061K93	\$83.94	order from McMaste
9" by 12" Instapak Quick Warmer (18 bag capacity)	1	SealedAir Corporation Catalog Number IQW0000-15	\$189.00	order from McMaste
Instapak Quick Foam Packaging bags	2 cartons of 48 bags	SealedAir Corporation Catalog Number IQH0000-10	\$263	Chiswick Trading
1" by 1" thick bass wood blocks	5 pieces, 1 ft long each		\$10	Pearl Arts & Crafts
3000 ml Beaker with 50 ml increments	1	McMaster Carr Catalog Number 9896T4	\$7.92	order from McMaste
		TOTAL	\$553.90	

¹ “Cellular Plastics”, *Handbook of Industrial Materials*, 2nd ed., Elsevier Advanced Technology, Oxford UK, 1992, pp. 540-545

² Brown, R.P, “Instrumented Tests”, *Handbook of Plastics Test Methods*, 3rd ed., Longman Scientific and Technical, New York, Wiley, 1998, pp. 160-161

³ Gardinier, Yanagihara, Kobayashi, Amito, “Design and Testing of the HOPE-X HSFD-II Landing System”, *AIAA Journal*, Vol. 20, No. 48, 2001, pp. 304-310

⁴ G. Brown, R. Haggard, R. Benney , “Parachute Retraction Soft Landing Systems Using Pneumatic Muscle Actuators”, *AIAA Journal*, Vol. 43, No. 8, 2000, pp. 1-9